Structural studies of argon-sputtered amorphous carbon films by means of extended x-ray-absorption fine structure

G. Comelli,* J. Stöhr, C. J. Robinson,† and W. Jark‡
IBM Research Division, Almaden Research Center, San Jose, California 95120-6099
(Received 11 April 1988)

The temperature-dependent microscopic structure of plasma-deposited *a*-C:H and magnetron-sputtered *a*-C films, *in situ* sputter cleaned by argon bombardment, has been investigated by near-edge (NEXAFS) and extended (EXAFS) x-ray-absorption fine-structure studies. We find that the microscopic structure of the two films becomes indistinguishable after sputtering with a loss of hydrogen for the *a*-C:H sample. The structure of the sputtered films at 30 °C is characterized by a first-neighbor C—C bond length of 1.445(10) Å. Upon annealing the bond length approaches that of graphite (1.421 Å) with a value of 1.427(10) Å at 1050 °C, the highest annealing temperature used. Analysis of the EXAFS amplitude of the first-neighbor shell leads to a two-phase structural model consisting of a "graphitelike" network and a statically and dynamically disordered "random matrix." The fraction of carbon atoms in the "graphitelike" network increases from 60(6)% at 30 °C to 92(9)% at 1050 °C. Analysis of the higher-neighbor-shell EXAFS signals leads to a model for the "graphitelike" regions, consisting of a network of conjugated odd- and even-membered rings, without long-range order. In contrast, the "random matrix" is suggested to be a mostly chainlike network of double and single bonds. Our results suggest that the "graphitelike" matrix is a precursor state for crystallization.

I. INTRODUCTION

The determination of the microscopic structure of amorphous carbon (*a*-C) and hydrogenated amorphous carbon (*a*-C:H) films is of considerable interest because of the technological importance of such materials.[1–3] Thin films of these materials exhibit a variety of properties which can be varied according to the deposition techniques used. For example, *a*-C films prepared by sputtering are electrically conducting and show high optical absorption at visible wavelengths. In contrast, by introducing hydrogen into the matrix a band gap is produced and the films become electrically insulating and transparent in the ir and mid-visible spectral regions. The characteristics of high hardness, optical transparency, high refractive index, and chemical inertness of these *a*-C:H films have historically led to the terminology "diamondlike" to describe their bonding. As a consequence of their properties, such films have found applications as protective coatings and optical coatings for ir sensors. Since all of these films are amorphous in structure, it is a misleading terminology, however, to refer to the bonding as diamondlike. Indeed, within the amorphous network of these materials many bonding configurations are possible and it is more likely that the atomic structure is made up of distributions of bonds comprising varying degrees of hybridization.

Carbon readily forms sp^3, sp^2, and sp^1 bonds, each of which may occur to varying extents in these films depending, for example, on deposition conditions and hydrogen content. The C-C nearest-neighbor distance, the coordination number, and the C—C—C bond angle are expected to differ significantly from one configuration to the other. For the unhydrogenated films one might expect configurations similar to those in the two crystalline configurations of carbon, diamond, and graphite. In sp^3-hybridized diamond each carbon atom is tetrahedrally coordinated (109.5° bond angle) with a bond length of 1.544 Å, while in sp^2-hybridized graphite the bonding is planar and trigonal (120° bond angle) with a bond length of 1.421 Å. In the presence of hydrogen a myriad of bonding configurations can be imagined with bond lengths ranging from 1.20 Å (triple bond) to 1.55 Å (single bond) and bond angles from 180° (e.g., two unsaturated adjacent C—C bonds) to 60° (as in cyclopropane), although bond angles in the 110°–130° range are most likely.[4,5]

Several experimental techniques have been used in order to investigate the microscopic bonding and structure in *a*-C and *a*-C:H films and in related materials such as glassy carbon. A review of this work has recently been published by Robertson.[2] Despite all this effort, the microscopic structure is far from being understood. Because of its local character the extended x-ray-absorption fine-structure (EXAFS) technique[6] is, in principle, well suited for structural studies of disordered systems and it has been extensively applied to the study of amorphous materials,[7] in general, and to covalent (hydrogenated) amorphous semiconductors like Si (Ref. 8) and Ge (Refs. 8–11), in particular, EXAFS has also been used to investigate *a*-C and *a*-C:H films,[12–15] but because of the limited EXAFS range available and lack of experimental C-C phase-shift data, a quantitative analysis of the data has not been performed.

In this paper we present near-edge x-ray-absorption fine-structure (NEXAFS) and EXAFS measurements of

a-C and *a*-C:H films which were *in situ* argon-sputtered to eliminate surface contamination. Data were recorded at room temperature as a function of annealing temperature up to 1050 °C. Our EXAFS data extend to more than 500 eV above the C *K* edge (284 eV) and are compared with those of graphite and diamond, which served as model systems. Our study shows that the sputtered films consist of "graphitelike" regions embedded in a "random matrix" of truly disordered (amorphous) material. The "random matrix" is mainly composed of a statically (single and double bonds) and dynamically (Debye-Waller factor) disordered chainlike network, while the "graphitelike" regions consist of a network of odd- and even-membered conjugated rings. During the annealing process the number of carbon atoms in the "graphitelike" regions is found to grow even though there is always a lack of long-range order. The percentage of carbon atoms in the "graphitelike" regions at the different stages of the annealing process is estimated to vary from 60% at room temperature to 92% at 1050 °C.

II. EXPERIMENT

Thin films ($\simeq$500 Å) of *a*-C:H on Si(111) were prepared using plasma deposition from methane in a conventional rf-diode apparatus.[16–18] The hydrogen content in these films was measured using nuclear-reaction analysis and was about 40 at. %. We also studied *a*-C thin films made by dc planar magnetron sputtering. The films were prepared at IBM and exposed to atmosphere before they were inserted into the measurement chamber at Stanford. In order to remove surface oxygen contamination the samples were argon-sputtered *in situ* at a pressure of 5×10^{-5} Torr for about 30 min at 500 V and at 1 keV accelerating voltage, respectively. The amount of oxygen on the surface dropped drastically in the first 15 min of the sputtering treatment, after which it did not diminish anymore. As will be discussed later, the sputtering treatment provoked structural changes in the thin films. In fact, the two samples became nearly indistinguishable and there was no evidence for hydrogen in the *a*-C:H sample after the sputtering. For this reason we will refer to both samples simply as *a*-C. NEXAFS and EXAFS measurements were made at room temperature on both samples before annealing and on the *in situ* sputtered *a*-C:H sample after annealing for 30 s to 720, 900, and 1050 °C, respectively. The preparation of the graphite and diamond samples has been reported before.[19]

The measurements were performed using the grasshopper monochromator (1200 lines/mm holographic grating) on beam line I-1 at the Stanford Synchrotron Radiation Laboratory. The NEXAFS and EXAFS spectra were recorded by total-electron-yield detection.[20] The spectra of the *a*-C films and the diamond single crystal were recorded at normal x-ray incidence on the sample (E parallel to the surface). The normal-incidence geometry was chosen out of convenience and because the nature of the samples renders the EXAFS amplitude independent of x-ray-incidence angle. This was confirmed by the fact that NEXAFS spectra from the *in situ* sputtered *a*-C:H sample revealed no angular dependence, in accordance with the expected disordered nature of the sample. The tetrahedral symmetry of diamond eliminates polarization-dependent effects, *per se*.[21] For the highly oriented pyrolitic graphite sample an x-ray-incidence angle of 55° from the basal plane ("magic angle") was used in order to eliminate polarization-dependent effects on the EXAFS amplitude. Both the diamond and the graphite sample had been used in a previous EXAFS study.[19] All spectra were normalized by the signal from a metal-grid reference monitor which eliminated possible time-dependent instabilities of the x-ray flux from the storage ring and by the independently recorded signal from a clean Si wafer which was used to eliminate energy-dependent structures in the monochromator transmission function, as discussed previously.[19,22,23]

III. NEXAFS RESULTS AND INTERPRETATION

In Fig. 1 we compare the NEXAFS spectra of the sputtered *a*-C sample at room temperature (RT) with graphite

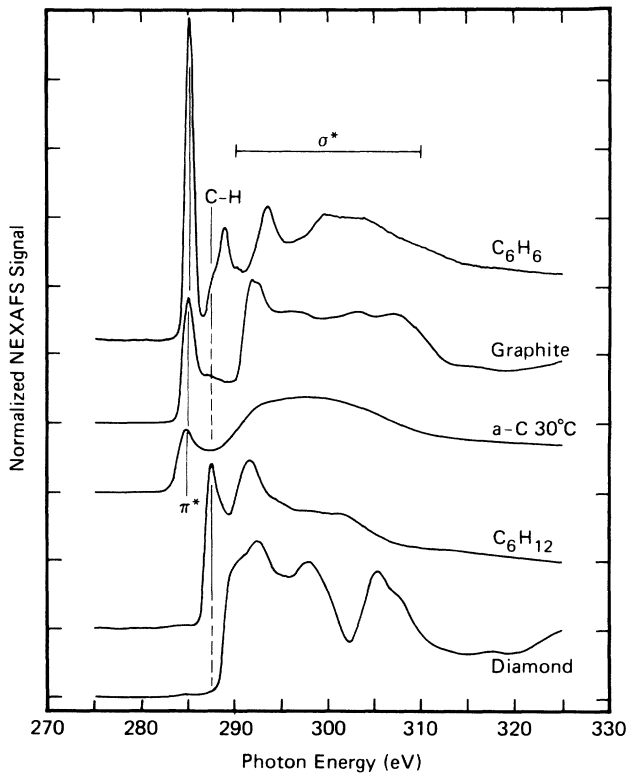

FIG. 1. C *K*-shell NEXAFS spectra of various molecules and solids as indicated. The benzene (C_6H_6) and cyclohexane (C_6H_{12}) spectra were recorded for condensed films at 80 K. The graphite spectrum is that of a highly oriented pyrolytic sample (monochromator graphite) recorded with the x-ray **E** vector at a 55° "magic" angle with respect to the *c* axis, in order to eliminate polarization-dependent effects. The resonance labeled π^* corresponds to a transition to π^* antibonding orbitals. Between 290 and 310 eV transitions to σ^* antibonding orbitals, or σ^* bands in case of the solids, are observed, as indicated. In the hydrocarbons a C-H resonance is observed at 287.5 eV, especially visible for cyclohexane. The assignment of the resonances follows that of Outka and Stöhr (Ref. 24).

and diamond,[19,24] and condensed films of benzene (C_6H_6) and cyclohexane (C_6H_{12}).[23,24] The spectra shown are in good agreement with those reported earlier in the literature for crystalline graphite,[25] diamond,[26,27] benzene,[28] cyclohexane,[29] and disordered carbon films.[14,15,30] The assignment of the various features in the K-shell absorption spectra has also been discussed in these previous papers and the labeling in Fig. 1 reflects that assignment. The presence of a π^* resonance at 285 eV is characteristic of unsaturated (sp or sp^2) carbon bonds. Its prominent intensity in the a-C sample therefore indicates the presence of unsaturated bonds as in benzene and graphite, but in contrast to cyclohexane and diamond. In linear hydrocarbons the energy position of the σ^* resonance provides a sensitive measure of bond lengths and therefore bond hybridization, varying from 291 eV for single bonds to 310 eV for triple bonds.[31,32] In aromatic rings or in solids, interactions of adjacent bonds cause a splitting of the resonances through conjugation or long-range band formation, and the simple correlation between bond length and resonance position is lost.[24] The structureless, broad σ^* feature for a-C arises from a superposition of the signatures of many different bonding configurations in the matrix. Its position and width (also see Fig. 2) indicates that there is no significant sp-bonded component which would give rise to a σ^* intensity around 310 eV. It is interesting to note that there is no structure in the spectrum of the RT a-C sample corresponding to the C—H resonance present both in the benzene and cyclohexane spectra. This can be interpreted as a first indication that the *in situ* sputtering eliminated the hydrogen from the film, *vide infra*.

In Fig. 2 we show the NEXAFS data as a function of annealing temperature and compare them to those of graphite. It is evident that with increasing annealing temperature the spectra become more graphitelike: the π^* resonance grows, indicating a growing number of unsaturated bonds, while structures appear in the σ^* region, indicating increasing structural order in the sample. It is important to note, however, that even after annealing to 1050 °C the NEXAFS spectrum of a-C is still significantly different from graphite. The lack of pronounced structure in the σ^* region indicates that the structural transformation in the film has not created a unique short- or long-range order. Either the matrix is heterogeneous and only a fraction of the atoms are part of a well-defined structure (e.g., small crystallites), or the matrix is homogeneous, but the network does not exhibit long-range periodicity. Unfortunately, for our isotropic bulk samples, NEXAFS only provides a qualitative picture of the structure changes.

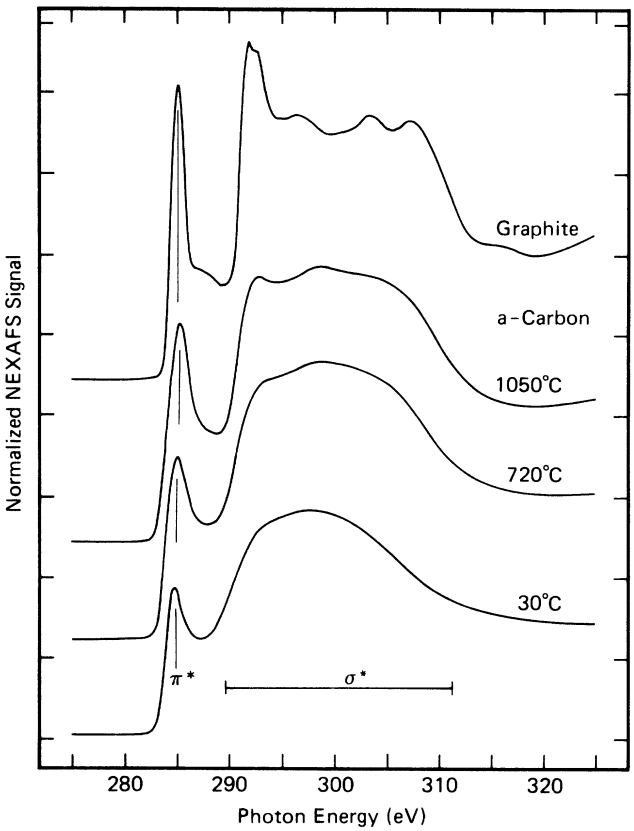

FIG. 2. NEXAFS spectra of a plasma-deposited a-C:H film on Si, which was *in situ* argon-sputtered, and is denoted "a-Carbon." Spectra were recorded at 30 °C after temporary anneals of the film to the indicated temperatures. For comparison, the spectrum of graphite recorded at the magic angle is shown on top.

IV. EXAFS RESULTS AND ANALYSIS

A. Overview of experimental results

In order to understand the microscopic structural changes in more detail, it is necessary to analyze the EXAFS region of the absorption spectra. Even after sputtering, the EXAFS spectra of the RT and 720-°C annealed samples revealed the presence of some residual oxygen contamination through the presence of a K-edge jump at about 540 eV. The size of the oxygen K-edge jump, however, was very small compared to that of the C K edge, being 3% and 1%, respectively, at RT and 720 °C. Therefore it was possible to remove the oxygen contribution simply by subtracting an appropriate step function from the two spectra. A simple step function is sufficient because the EXAFS due to oxygen is negligible (1–3 %) relative to that due to bulk carbon. After annealing to 900 and 1050 ° no oxygen edge jump was present in the spectra. In the following we shall only show and discuss data where the spurious oxygen contribution, if present, has been subtracted. Figure 3 shows the normalized EXAFS signals of the a-C sample as a function of annealing temperature, and those of graphite and diamond, for comparison. All data were processed by using the same normalization procedure, i.e., subtraction of a spline polynomial and normalization to the edge jump. This ensures that the amplitude of the oscillations is normalized to the total number of carbon atoms in the x-ray beam. The a-C spectra displayed in Fig. 3 refer to the *in situ* sputter-cleaned a-C:H sample, but, as shown in Fig. 4, the EXAFS signal from the magnetron-sputtered a-C

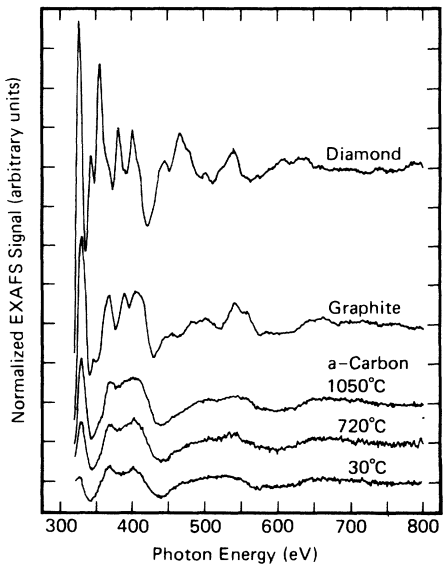

FIG. 3. EXAFS signals of diamond, graphite (recorded at the magic angle), and the "*a*-Carbon" sample after annealing to different temperatures. The EXAFS signals were obtained from the raw data by subtraction of a spline-polynomial background and normalization to the edge jump and are plotted vertically offset on the same scale.

film, subjected to the same *in situ* cleaning procedure, yielded a nearly indistinguishable spectrum. Note that raw data are compared in Fig. 4 and that the small differences would disappear almost entirely upon background correction. This indicates that the *in situ* sputtering process is responsible for the microscopic structure of the measured films, and, in the case of the *a*-C:H sample, leads to a depletion of C—H bonds.

Without detailed analysis, some important conclusions can be drawn from the EXAFS signals in Fig. 3. First, it is apparent that for all *a*-C spectra the fundamental frequency of the EXAFS is closer to graphite than to diamond. For example, the diamond signal has a maximum around 620 eV while the graphite and *a*-C signals exhibit a minimum. It is evident, however, that the EXAFS of graphite contains more (higher) frequencies than that of *a*-C. During the annealing process two main changes occur with increasing temperature: (i) the higher-frequency structure, especially at the lowest energies, becomes more pronounced, and (ii) the overall size of the EXAFS amplitude increases. The largest effect is the growth of the single peak around 326 eV. We have previously shown for graphite[19] that this peak cannot be accounted for by the conventional single-scattering EXAFS theory, and it was therefore excluded from the energy range used for the graphite analysis. Multiple-scattering calculations for graphite by Vvedensky[33] indicate that the intensity of this peak appears to be related to the microscopic short-range order in the sample. The peak is absent for the nearest-neighbor distance, first appears when the second-shell contribution is added, and is nearly fully developed when all shells within 4 Å are taken into account. The other effect of the annealing process, i.e., the increase of the overall EXAFS amplitude, occurs equally at all energies. This is best visualized by inspection of Fig. 5, where we have superimposed the EXAFS signal of graphite and of the RT *a*-C sample. The latter spectrum has been normalized by eye to the graphite one, using a multiplicative factor of 1.8. It is evident that the overall EXAFS amplitude in *a*-C at RT relative to graphite is simply reduced by this energy-independent constant factor.

In order to extract physical parameters from the EXAFS signals, the energy scale was converted to wave-vector scale, using the absorption edge of graphite, 284 eV, as the "zero" of energy. We then Fourier-transformed the data in the range 350–750 eV ($4 \leq k \leq 11$ Å^{-1}) after weighting by k^2 and multiplying by a window function to minimize data-truncation effects. The resulting magnitude of the Fourier transforms for the different spectra are shown in Fig. 6(a). The position and width of the first two peaks in $|F(r)|$ is almost exactly the same for all cases. These peaks are related to the three C-C distances within the six-membered ring. The first-neighbor C-C distance (1.421 Å) corresponds to the first peak, while the second (2.461 Å) and third (2.842 Å) C-C distances cannot be resolved and contribute to the second peak. Another interesting point is that there are no

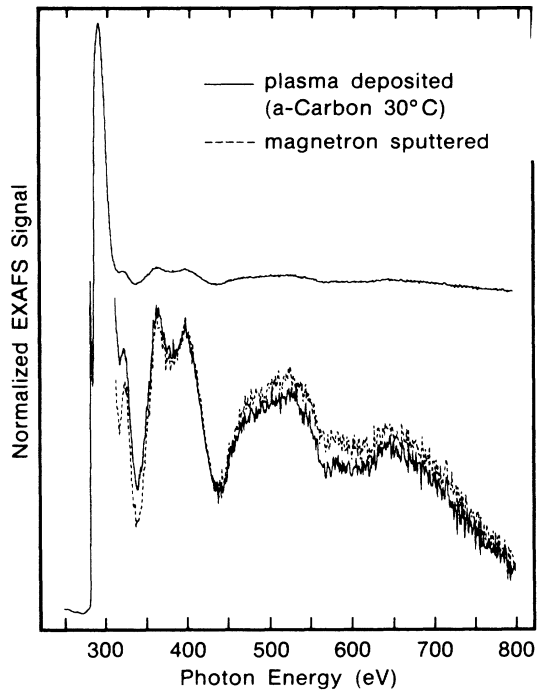

FIG. 4. Comparison of the raw EXAFS data recorded for the plasma-deposited *a*-C:H film and a magnetron-sputtered *a*-C film, after both were subjected to the same *in situ* argon-sputtering treatment. The spectrum shown (solid line) is that used to generate the EXAFS signal at the bottom of Fig. 3. The two EXAFS signals shown would become nearly indistinguishable after processing the data with standard background-subtraction procedures that would eliminate long-wavelength components arising from instrumental drifts and other experimental factors.

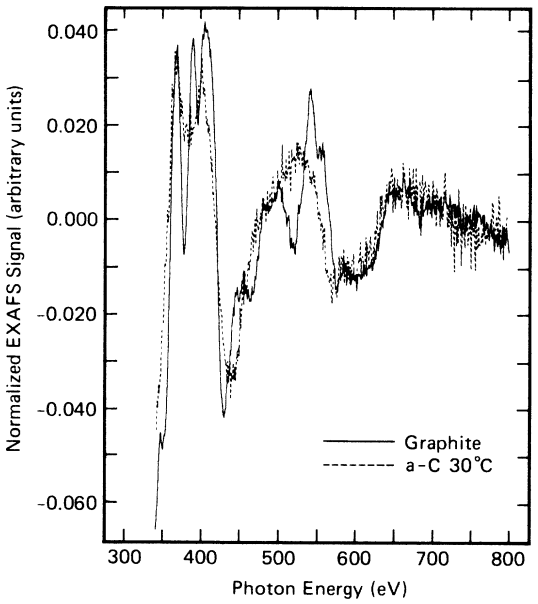

FIG. 5. Comparison of the EXAFS signals of graphite (magic angle) and the *in situ* sputtered plasma-deposited sample (denoted "*a*-C 30 °C") after background subtraction and normalization to the edge jump. The amplitude of the *a*-C signal has been multiplied by a factor of 1.8. Note that both amplitudes show the same decrease with energy.

significant peaks in the *a*-C transforms corresponding to distances larger than the third-nearest-neighbor intraring distance (2.842 Å), while the EXAFS of graphite contains contributions of shells as far as 6 Å from the absorbing C atom. Note that we have ignored the third peak in the *a*-C 30-°C transform at 2.9 Å in our above discussion because it was found to be sensitive to the subtraction of the O *K*-edge background and hence we are not sure that it is physically meaningful. The first two peaks in the transforms increase with increasing annealing temperature and approach those of graphite, especially the first peak. In Fig. 6(b) the same Fourier transforms, $|F(r)|$, normalized to the height of the first peak are shown, which emphasizes the slower growth of the second- and third-shell signals with temperature relative to that of the first shell. In fact, the second peak remains constant between 720 and 1050 °C. Below we shall discuss the quantitative analysis of the data.

B. Analysis of first-neighbor shell: Need for a two-phase model

Using the C-C phase shift previously determined from graphite,[19] we can obtain the C-C nearest-neighbor distances for the different cases from the first peak in $|F(r)|$. The results are reported in Table I and are found to be close but not identical to the value for graphite, 1.421 Å. The small but systematic decrease of the de-

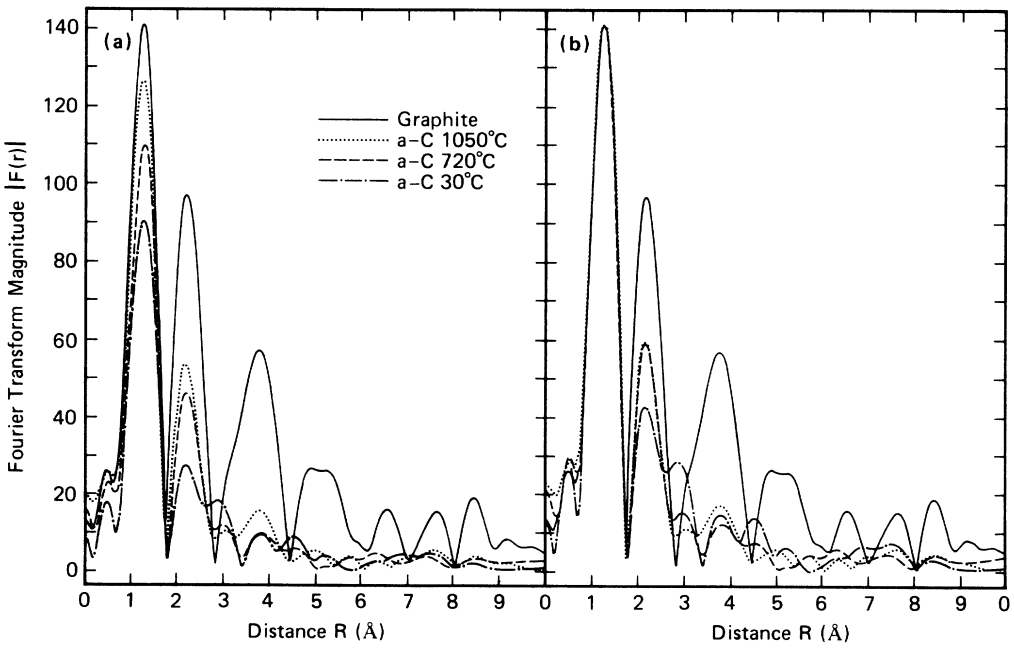

FIG. 6. (a) Absolute magnitude of the Fourier transforms of the EXAFS signals shown in Fig. 3 (350–750 eV) for the *a*-C film annealed to different temperatures and graphite. Note the increase with annealing temperature of the first- and second-transform peaks corresponding to the first- and the combined second- and third-C-C-neighbor distances, respectively. Also note absence of higher-neighbor-shell peaks for *a*-C at all temperatures. (b) Same as (a), but all transforms normalized to the height of the first-transform peak. This shows the slower growth of the second- than the first-transform peak with temperature.

TABLE I. First-shell parameters for *a*-C sample.

	C-C distance[a] (Å)	"Graphitelike" fraction (%)
a-C 30 °C	1.445(10)	60(6)
a-C 720 °C	1.441(10)	80(8)
a-C 900 °C	1.429(10)	87(9)
a-C 1050 °C	1.427(10)	92(9)

[a]Using graphite with $R = 1.421$ Å as our standard.

rived C—C bond lengths towards the graphite value with increasing annealing temperature is indeed meaningful. EXAFS data of good signal-to-noise level and a data range extending to $k > 10$ Å^{-1} typically give first-nearest-neighbor distances within ±0.01 Å, independent of the analysis procedure. The accuracy of the result then hinges on the reliability of the phase-shift–transferability procedure.[6] In our case, the graphite model and the *a*-C sample are so similar that the phase shifts should be identical and not introduce any additional error. This has been checked previously by comparing the EXAFS of graphite and diamond.[19] Thus the listed distances in Table I are reliable to <0.01 Å and indicate that with increasing annealing temperature the nearest-neighbor distance becomes slightly shorter and approaches graphite at the highest temperatures.

Any microscopic structural model for *a*-C has to fulfill three criteria for the first-neighbor shell imposed by our data: (i) a C—C bond length around 1.42 Å, (ii) a *k*-dependent EXAFS amplitude close to graphite, and (iii) an overall amplitude reduction relative to graphite which decreases with annealing temperature. In order to explore the implications of various structural models on the C-C nearest-neighbor EXAFS signals, we performed model-dependent EXAFS simulations using single-scattering EXAFS theory. We employed the graphite C-C phase shift,[19] but ignored the damping terms and the C-C backscattering amplitude function, since we are only interested in comparing the amplitudes of the calculated EXAFS signals for different models to that of the graphite standard. In Fig. 7 we show the distribution of C-C distances for the models used, the calculated EXAFS signals, and their transforms $|F(r)|$. Model A takes into consideration only the C-C distance of graphite and serves as a reference for the other models, according to the three criteria given earlier. Model B describes a situation in which two different distinct bond lengths of equal abundance are present, namely C—C single (1.54 Å) and double (1.34 Å) bonds. Model C uses a continuous distribution of bond lengths from the double-bond to the single-bond value. Model D assumes two types of bonds, like model B, but with two differences. First, the number of double bonds is half the number of single bonds, as suggested by a previous study of hydrogenated amorphous carbon films.[14] Secondly, the possibility of deviations from the "ideal" bond lengths is taken into account. Our distribution in distances is taken from the range of values for molecular hydrocarbons with a mixture of single and double bonds. In such molecules bond-conjugation effects lead to a larger spread in "single-bond" than "double-bond" distances similar to that assumed for model D.[5]

It is evident that none of the models B–D satisfies all of our criteria. The EXAFS signal either shows an energy-dependent amplitude modulation due to two different bond lengths, an energy-dependent amplitude reduction due to a distribution in bond lengths (similar to a Debye-Waller factor), or a peak in $|F(r)|$ which is shifted from the correct position. We tried many variations of model D with different mixtures of single and double bonds. By varying the distribution and relative number of two types of bonds, we could never obtain both an energy-independent amplitude-reaction factor and the correct position of the peak in $|F(r)|$. The only model which gives the proper C-C distance and a nearly energy-independent amplitude function is that labeled E in Fig. 7. This model uses a distribution of values around

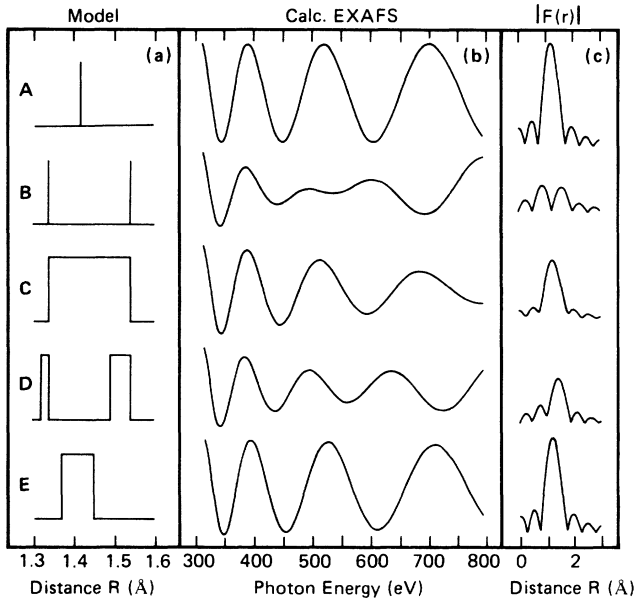

FIG. 7. Model calculations of the EXAFS signal for different C—C bonding configurations. The models A—E are shown in column (a), the calculated EXAFS signal in (b), and the corresponding Fourier-transform magnitude $|F(r)|$ in (c). Model A represents the case of graphite and serves as a standard for the observed energy dependence of the EXAFS amplitude and the average bond length obtained from $|F(r)|$. Model B assumes a mixture of equally abundant discrete C—C single ($R = 1.54$ Å) and double ($R = 1.34$ Å) bonds, while model C assumes a continuous distribution of bond length in between those values. Model D allows for a distribution around the double- ($1.32 \leq R \leq 1.34$ Å) and single- ($1.49 \leq R \leq 1.54$ Å) bond values with half the number of double than single bonds. The distribution uses the fact known from hydrocarbons (Ref. 5) that conjugation shifts the average length of "single" bonds to lower values and causes a larger spread in bond lengths relative to double bonds. Model E assumes a distribution of bond lengths ($1.37 \leq R \leq 1.45$ Å) around the value in graphite.

the C-C distance of graphite and gives an EXAFS signal and $|F(r)|$ very similar to those of model A.

The EXAFS frequency and the energy dependence of the amplitude thus leads to a "graphitelike" microscopic structural model. However, one striking result obtained from our data remains unexplained: the overall reduction in EXAFS amplitude which gradually disappears with increasing annealing temperature as revealed by the data in Fig. 3 and the transforms shown in Fig. 6. The *energy independence* of the observed amplitude reduction cannot be explained by a single phase of connected rings which is homogeneous over macroscopic dimensions. For a homogeneous matrix an *energy-independent* amplitude reduction relative to graphite could only occur if the average coordination number of carbon was reduced below three. At 30 °C the EXAFS amplitude is only 60% that of graphite, which formally corresponds to an average coordination number of 2 per carbon atom and is therefore unphysical. Note that static and/or dynamic disorder in the nearest neighbor C—C bonds would lead to an *energy-dependent* amplitude reduction, which is in disagreement with the comparison shown in Fig. 5. Therefore, we need to postulate the coexistence of two phases which differ significantly in their microscopic structure. We suggest that one region is a "random matrix," in which all possible C—C bonds are present particularly chainlike units together with dangling bonds.[34] The second region is "graphitelike" and has a distance distribution around 1.42 Å in between models A and E. We shall discuss this structure in more detail later after considering the implications of the two-phase model. The random matrix does not generate a relevant EXAFS signal in the range $k > 4$ Å^{-1} because of the presence of a high static and dynamic disorder. Both the larger distribution in bond lengths and the larger Debye-Waller factor quench the EXAFS signal at high k. Here we point out that the in-plane Debye temperature of graphite is very high ($\sim$1300 K),[35] and thus ringlike units, especially when made more rigid by conjugation, are expected to have significantly smaller mean-square relative displacements than chainlike units, which are suggested to dominate in the random matrix. This is confirmed by EXAFS studies of polymers. For example, polybutadiene, which contains chains with a mixture of single and double bonds, exhibits an EXAFS amplitude that is less than half the amplitude of the a-C sample at 30 °C.[36] For our model the measured EXAFS amplitude can be explained as follows. Atoms in the "random matrix" contribute to x-ray absorption and therefore contribute to the measured jump at the C K edge. They do not give rise to a sizable EXAFS signal, however, in the k range (> 4 Å^{-1}) used for the present analysis. Since in the analysis procedure the EXAFS signal is normalized to the edge jump, i.e., to the number of absorbing atoms, a reduction in amplitudes is observed which is proportional to the relative number of atoms in the "random matrix." With the annealing process more C atoms pass from the "random matrix" to the "graphitelike" regions, and the EXAFS amplitude grows as discussed quantitatively below.

Our two-phase model is similar to that proposed by Stern *et al.*[10] from their EXAFS analysis of amorphous Ge. In that case the model was derived from analysis of the second-shell EXAFS signal since opposite to carbon the first-nearest-neighbor shell in crystalline and amorphous Ge is identical in distance and coordination. The second-shell signal is sensitive to disorder which affects the tetrahedral bond angle. Bond-angle distortions lead to a distribution in second-nearest-neighbor distances and, also, to a larger mean-square relative displacement of second-nearest neighbors.[10]

The fraction of atoms in the two phases at the various annealing stages can be obtained from the EXAFS amplitude of the first shell in a-C relative to that in graphite. It is directly given by the ratio of the area of the first peak in $|F(r)|$ in a-C relative to graphite, or can be obtained by a detailed analysis of the amplitude ratio in a k-dependent plot.[6] We investigated the reliability of the two methods for our case by comparing two EXAFS spectra of single-crystal graphite, recorded at two orientations of the c axis relative to the electric field vector of the x rays, i.e., 90° (normal incidence) and 55° (magic angle). From theory one would expect a ratio of 1.5 between the effective coordination numbers.[21] With the k-dependent amplitude-ratio method we obtained a factor of 1.64, while the peak-area method yielded 1.46, in better and satisfactory agreement with theory. The larger error for the k-dependent amplitude-ratio method is due to the fact that the decay of the C backscattering amplitude with increasing energy and the short C-C distance, giving rise to only few EXAFS oscillations, cause a greater uncertainty in the slope of the amplitude ratio than in the peak area, which corresponds to a k-averaged amplitude. We therefore used the peak-area method for our amplitude analysis of the a-C data relative to graphite. Our analysis tacidly assumes that the Debye-Waller factors in the "graphitelike" phase of a-C and in graphite are the same. The comparison of the energy dependence of the amplitudes for a-C and graphite shown in Fig. 5 indicates that this is indeed a reasonable assumption. We find that the "graphitelike" component grows from 60(6)% at 30 °C to 92(9)% at 1050 °C. The results are summarized in Table I.

C. Analysis of higher-neighbor shells: Structure of the "graphitelike" network

The signature of the higher shells contains important information on the crystallographic structure of the "graphitelike" network. There are two simple intuitive models for the microscopic structure of the "graphitelike" phase. The first simply consists of graphite crystallites, the second of a network of rings, including five- and seven-membered rings. The temperature dependence of the EXAFS amplitude for the second- and third-neighbor shells and the absence of a higher-shell signal allows us to discard the first model.

Figure 6(b) reveals that when the first peak in $|F(r)|$ for the a-C samples is normalized to that of graphite, the second peak is still significantly reduced in intensity relative to that for graphite. This means that the disorder in the second- and third-nearest neighbor shells is significantly higher than in the first shell. Also, the relative amplitude of the second peak does not increase any

further after annealing to 720 °C. This is confirmed also by the data obtained after annealing to 900 °C, which are not shown. We know from analysis of the first-neighbor-shell amplitude that, after the final anneal to 1050 °C, 92% of the carbon atoms are in the "graphitelike" region of the matrix. This allows us to exclude a model based on graphite crystallites in an amorphous matrix. In such a model the second-neighbor peak in the transform would be reduced relative to the first one if the crystallites are small. Then the carbon atoms on the periphery of the small crystallites would have a distorted second and third coordination shell, leading to an EXAFS amplitude reduction. Simulations show that the strong reduction in the second- to first-peak ratio observed at 1050 °C (see Fig. 6) requires the graphite crystallites to be very small (less than five rings). Also, the missing peaks in the *a*-C transforms in Fig. 6, corresponding to neighbors in the fourth, fifth, etc. shells, are only compatible with a small size of the crystallites. The small size, however, leads to an unphysical result in that it is inconsistent with the fact that only 8% of the atoms occupy the connecting random network. For example, for a microcrystal composed of a symmetric arrangement of seven six-membered rings, i.e., a total of 24 carbon atoms, half of the atoms are left with open bonds. Thus the interconnection of such microcrystals would require a large fraction of atoms in disordered bridging positions, even if the void density is assumed to be as high as several percent.

We are led to the conclusion that the "graphitelike" network must contain non-six-membered rings which cause the reduction in the second- and third-shell amplitudes through a simple distribution in higher-neighbor-shell distances. The constancy of the second peak in Fig. 6(b) in the (720–1050)-°C range indicates that the formation of new six-membered rings is accompanied by the formation of non-six-membered rings in the same proportion, so that the static disorder for the higher shells remains constant. At even higher temperatures the "graphitelike" network will eventually convert into graphite. The presence of odd-membered rings also explains the missing EXAFS signal from higher-neighbor shells in Fig. 6 since the static disorder due to the presence of these non-six-membered rings grows dramatically the further the neighbor shell is separated from the central atom. Odd-membered rings can play the role of connecting elements between the planar aromatic rings, allowing a randomly oriented network of rings as recently suggested by Van Vechten and Keszler.[37] Such linking of odd- and even-membered rings has molecular analogues in indenyl (C_9H_7) (Ref. 38) or indene (C_9H_8) (Ref. 5) consisting of joined five- and six-membered rings with an average C—C bond length of 1.42(1) Å or azulene ($C_{10}H_6$),[5] consisting of joined five- and seven-membered rings and an average C—C bond length of 1.40 Å. Thus the C—C bond-length distribution expected for a strongly conjugated connecting-ring structure is indeed centered around the 1.42-Å value of model E in Fig. 7.

V. SUMMARY AND CONCLUSIONS

Our NEXAFS results can be summarized as follows. The sputtered films contain a significant fraction of sp^2 hybridized carbon bonds as revealed by the presence of a prominent π^* resonance. With increasing annealing temperature this resonance grows, indicating the formation of an increasing number of unsaturated C—C bonds. The σ^* resonance or band region is largely structureless at 30 °C, which is attributed to a distribution in bonding configurations in the film. The presence of a significant fraction of *sp*-hybridized carbon is excluded from the position and width of the σ^* feature. Even after annealing to 1050 °C the σ^* region remains rather structureless relative to graphite or diamond, indicating the absence of long-range order in the film.

The EXAFS data yield a more quantitative structural picture. The C—C bond length in the film is found to be within 0.025 Å that of graphite (1.421 Å) at all annealing temperatures used. In contrast, the bond length is shorter by more than 0.10 Å than that in diamond (1.544 Å). This shows that the films are more "graphitelike" than "diamondlike" in structure. A reduction of the first-neighbor-shell EXAFS amplitude for *a*-C relative to graphite leads to a two-phase structural model consisting of a "graphitelike" network and a "random matrix." The "random matrix" is suggested to consist of different kinds of C—C bonds, in particular, chainlike units and dangling bonds, and it is characterized by a high static and dynamic disorder. With increasing annealing temperature the amplitude of the nearest-neighbor EXAFS signal reveals a growth of the "graphitelike" fraction from 60% at room temperature to 92% at 1050 °C. Analysis of the higher-neighbor-shell EXAFS leads to a model for the "graphitelike" regions in terms of a network of conjugated even- and odd-membered rings.

The qualitative structural picture of the sputtered *a*-C films revealed by the NEXAFS data is quantitatively confirmed by the EXAFS results which allow us to derive a model for the microscopic structure of the films. Our model suggests a unique crystallization process for graphite from a truly disordered matrix via a "precursor phase" consisting of a network of odd- and even-membered rings. The first-neighbor coordination in this second "graphitelike" phase is well defined in terms of distance (1.42 Å) and coordination (3), but the distribution in the C—C—C bond angles and the different spatial orientation of the ring planes leads to a lack of intermediate and long-range order. In this sense the "graphitelike" phase is similar to the situation encountered in amorphous Si and Ge. The unique bonding properties of carbon complicate the amorphous to crystalline transition relative to *a*-Si or *a*-Ge in that there are two phases which could be called amorphous, the "random matrix" and "graphitelike" phases. Starting from a random chainlike network containing single and double bonds of different length, thermal bond activation leads to the formation of stable heavily conjugated even- and odd-membered rings with an average bond length intermediate between the single- and double-bond values. This network lacks medium- and long-range order. The conversion to crystalline graphite at temperatures well above 1000 °C is envisioned as a growth of the six-membered-ring component in the network of even- and odd-membered rings.

ACKNOWLEDGMENTS

We would like to thank D. A. Outka for help with the measurements, M. Le and K. K. Kim for providing the thin-film samples, and E. A. Stern for bringing the two-phase model for Ge to our attention. The experiments were carried out at the Stanford Synchrotron Radiation Laboratory, which is supported by the Office of Basic Energy Sciences of the U.S. Department of Energy and the Division of Materials Research of the National Science Foundation.

---

*Present address: Sincrotrone Trieste, Padriciano 99, I-34012 Trieste, Italy.

†Present address: Research Division, Raytheon Company, 131 Spring Street, Lexington, MA 02173.

‡Present address: Fritz-Haber-Institut der Max-Planck-Gesellschaft, Faradayweg 4-6, D-1000 Berlin 33, Federal Republic of Germany.

[1]J. A. Woollam, H. Chang, and V. Natarajan, Appl. Phys. Commun. **5**, 263 (1985-86).

[2]J. Robertson, Adv. Phys. **35**, 317 (1986).

[3]Hsiao-chu Tsai and D. B. Bogy, J. Vac. Sci. Technol. A **5**, 3287 (1987).

[4]A. F. Wells, *Structural Inorganic Chemistry* (Oxford University Press, Oxford, 1975), Chap. 21.

[5]*Structure Data of Free and Polyatomic Molecules,* Landolt-Börnstein, New Series II (Springer, Berlin, 1976), Vol. 7.

[6]For reviews of EXAFS spectroscopy, see *EXAFS Spectroscopy, Techniques, and Applications,* edited by B. K. Teo and D. C. Joy (Plenum, New York, 1981); P. A. Lee, P. H. Citrin, P. Eisenberger, and B. M. Kincaid, Rev. Mod. Phys. **53**, 769 (1981); Boon K. Teo, *EXAFS: Basic Principles and Data Analysis,* Inorganic Chemistry Concepts 9 (Springer-Verlag, Heidelberg, 1986); *Principles, Applications, Techniques of EXAFS, SEXAFS, and XANES,* edited by D. C. Koningsberger and R. Prins (Wiley, New York, 1988).

[7]E. D. Crozier, J. J. Rehr, and R. Ingalls, in *X-Ray Absorption: Principles, Applications, Techniques of EXAFS, SEXAFS, and XANES,* edited by D. C. Koningsberger and R. Prins (Wiley, New York, 1988), p. 373.

[8]For a recent compilation of papers on the subject, see J. Phys. (Paris) Colloq. **47**, C8-349 (1986), and references therein.

[9]P. Rabe, G. Tolkiehn, and A. Werner, J. Phys. C **12**, L545 (1979).

[10]E. A. Stern, C. E. Bouldin, B. von Roedern, and J. Azoulay, Phys. Rev. B **27**, 6557 (1983).

[11]C. E. Bouldin, E. A. Stern, B. von Roedern, and J. Azoulay, Phys. Rev. B **30**, 4462 (1984).

[12]B. M. Kincaid, A. E. Meixner, and P. M. Platzman, Phys. Rev. Lett. **40**, 1296 (1978).

[13]P. E. Batson and A. J. Craven, Phys. Rev. Lett. **42**, 893 (1979).

[14]J. Fink, T. Müller-Heinzerling, J. Pflüger, A. Bubenzer, P. Koidl, and G. Crecelius, Solid State Commun. **47**, 687 (1983).

[15]D. Wesner, S. Krummacher, R. Carr, T. K. Sham, M. Strongin, W. Eberhardt, S. L. Weng, G. Williams, M. Howells, F. Kampas, S. Heald, and F. W. Smith, Phys. Rev. B **28**, 2152 (1983).

[16]L. Holland and S. M. Ojha, Thin Solid Films **38**, L17 (1976).

[17]L. Holland and S. M. Ojha, Thin Solid Films **58**, 107 (1976).

[18]A. Bubenzer, B. Dishler, G. Brandt, and P. Koidl, J. Appl. Phys. **54**, 4590 (1983).

[19]G. Comelli, J. Stöhr, W. Jark, and B. Pate, Phys. Rev. B **37**, 4383 (1988).

[20]J. Stöhr, R. Jaeger, J. Feldhuas, S. Brennan, D. Norman, and G. Apai, Appl. Opt. **19**, 3911 (1980).

[21]J. Stöhr, in *X-Ray Absorption: Principles, Applications, Techniques of EXAFS, SEXAFS, and XANES,* edited by D. C. Koningsberger and R. Prins (Wiley, New York, 1988), p. 443.

[22]D. A. Outka and J. Stöhr, J. Chem. Phys. **88**, 3539 (1988).

[23]G. Comelli and J. Stöhr, Surf. Sci. **200**, 35 (1988).

[24]D. A. Outka and J. Stöhr, in *Chemistry and Physics of Solids Surfaces,* Vol. 7 of *Springer Series in Surface Science,* edited by V. R. Vanselow and R. Howe (Springer, Heidelberg, 1988).

[25]R. A. Rosenberg, P. J. Love, and V. Rehn, Phys. Rev. B **33**, 4034 (1986).

[26]J. F. Morar, F. J. Himpsel, G. Hollinger, G. Hughes, and J. L. Jordan, Phys. Rev. Lett. **54**, 1960 (1985).

[27]J. F. Morar, F. J. Himpsel, G. Hollinger, J. L. Jordan, G. Hughes, and F. R. McFeely, Phys. Rev. B **33**, 1346 (1986).

[28]J. A. Horsley, J. Stöhr, A. P. Hitchcock, D. C. Newbury, A. L. Johnson, and F. Sette, J. Chem. Phys. **83**, 6099 (1985).

[29]A. P. Hitchcock, D. C. Newbury, I. Ishii, J. Stöhr, J. A. Horsley, R. D. Redwing, A. L. Johnson, and F. Sette, J. Chem. Phys. **85**, 4849 (1986).

[30]D. Denley, P. Perfetti, R. S. Williams, D. A. Shirley, and J. Stöhr, Phys. Rev. B **21**, 2267 (1980).

[31]A. P. Hitchcock, S. Beaulieu, T. Steel, J. Stöhr, and F. Sette, J. Chem. Phys. **80**, 3972 (1984).

[32]F. Sette, J. Stöhr, and A. P. Hitchcock, J. Chem. Phys. **81**, 4906 (1984).

[33]D. D. Vvedensky (unpublished).

[34]C. J. Robinson, M. G. Samant, J. Stöhr, V. S. Speriosu, C. R. Guarnieri, and J. J. Cuomo, Mater. Res. Soc. Symp. Proc. **90**, 133 (1987).

[35]R. Chen and P. Trucano, Acta Crsytallogr. Sect. A **34**, 979 (1978).

[36]G. Comelli and J. Stöhr (unpublished).

[37]J. A. Van Vechten and D. A. Keszler, Phys. Rev. B **36**, 4570 (1987).

[38]L. Schäfer, J. Am. Chem. Soc. **90**, 3919 (1968).